High-Yield Synthesis of Boron Nitride Nanoribbons *via* Longitudinal Splitting of Boron Nitride Nanotubes by Potassium Vapor

Alexander Sinitskii,*,† Kristopher J. Erickson,‡,§,⊥ Wei Lu,∥ Ashley L. Gibb,‡,§,⊥ Chunyi Zhi,# Yoshio Bando,¶ Dmitri Golberg,¶ Alex Zettl,*,‡,⊥ and James M. Tour*,∥,△

†Department of Chemistry, University of Nebraska—Lincoln, Lincoln, Nebraska 68588, United States, ‡Department of Chemistry and §Department of Physics, University of California at Berkeley, Berkeley, California 94720, United States, ⊥Materials Sciences Division, Lawrence Berkeley National Laboratory, Berkeley, California 94720, United States, ∥Department of Chemistry, Rice University, Houston, Texas 77005, United States, #Department of Physics and Materials Science, City University of Hong Kong, Kowloon, Hong Kong , ¶International Center for Materials Nanoarchitectonics (MANA), National Institute for Materials Science (NIMS), Tsukuba, Ibaraki 305-0044, Japan, and △Department of Materials Science and NanoEngineering and The Smalley Institute for Nanoscale Science and Technology, Rice University, Houston, Texas 77005, United States

ABSTRACT Boron nitride nanoribbons (BNNRs) are theorized to have interesting electronic and magnetic properties, but their high-yield synthesis remains challenging. Here we demonstrate that potassium-induced splitting of BN nanotubes (BNNTs) is an effective high-yield method to obtain bulk quantities of high-quality BNNRs if a proper precursor material is chosen. The resulting BNNRs are crystalline; many of them have a high aspect ratio and straight parallel edges. We have observed numerous few-layer and monolayer BNNRs; the multilayered ribbons predominantly have an AA′ stacking. We present a detailed microscopy study of BNNRs that provides important insights into the mechanism of the formation of BNNRs from BNNTs. We also demonstrate that the BNNTs prepared by different synthetic approaches could exhibit dramatically different reactivities in the potassium splitting reaction, which highlights the need for future comparison studies of BN nanomaterials prepared using different methods to better understand their preparation-dependent physical and chemical properties.

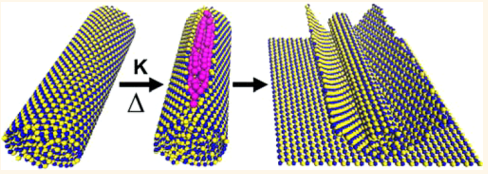

KEYWORDS: boron nitride nanotubes · potassium splitting · boron nitride nanoribbons

Boron nitride (BN) nanoribbons (BNNRs) are an emerging material with interesting theoretically predicted electronic and magnetic properties that depend on the ribbon width, edge structure, and termination.[1−9] According to other theoretical studies, the properties of BNNRs could be further tuned by the basal plane functionalization, such as hydrogenation.[10,11] However, the experimental verification of these theoretical predictions is challenging due to the absence of a scalable high-yield synthetic method that could produce BNNRs with specific width and edge properties.[12] Based on previously developed methods to produce graphene nanoribbons (GNRs) by unzipping carbon nanotubes (CNTs),[13−18] experimental studies focused on the synthesis of BNNRs similarly used boron nitride nanotubes (BNNTs) as a starting material.[19−21]

One of these reported approaches to prepare BNNRs is based on a longitudinal splitting of BNNRs caused by intercalation of potassium at 300 °C (Figure 1a).[20] As we demonstrated in our previous work,[20] this approach has several important advantages. First, the procedure is facile and scalable: a mixture of BNNTs and potassium is simply sealed in an ampule under vacuum and annealed at 300 °C for several hours. Second, the process yields BNNRs with many desirable properties, such as a high aspect ratio, uniform widths, and a minimal amount of defects in the basal plane as well as at the edges. However, the reported yield was quite low, which remains a significant drawback of the method; only ∼1% of treated BNNTs exhibited longitudinal splitting after the potassium vapor treatment.

Here we demonstrate that potassium-induced splitting of BNNTs could be used

* Address correspondence to sinitskii@unl.edu, azettl@berkeley.edu, tour@rice.edu.

Received for review August 26, 2014 and accepted September 16, 2014.

Published online September 16, 2014
10.1021/nn504809n

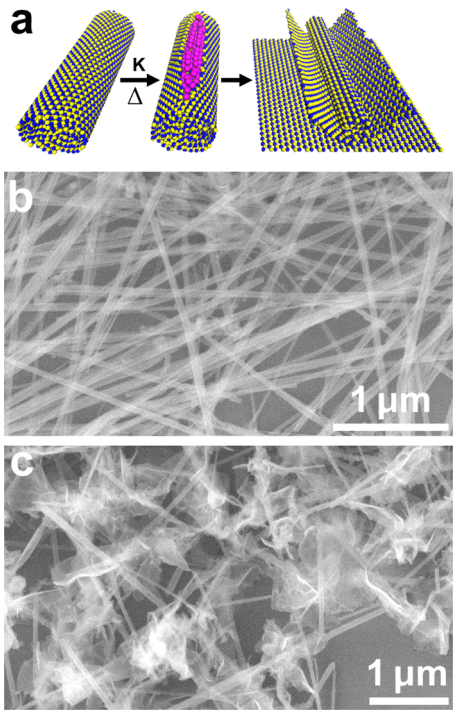

Figure 1. (a) Scheme of the unzipping of BNNTs to form BNNRs. Colors indicate different elements as follows: B, blue; N, yellow; K, pink. The potassium intercalation in the pristine BNNT (left) results in the local breaking of B−N bonds caused by the pressure buildup (middle), which progresses toward the complete longitudinal splitting of the nanotube to form a few-layer BNNR (right). (b) SEM image of pristine BNNTs. (c) SEM image of BNNRs formed by splitting BNNTs by potassium vapor at 300 °C for 72 h.

for the high-yield synthesis of BNNRs. In the original study, for the synthesis of BNNRs, we used BNNTs synthesized according to the previously reported procedure.[22] Briefly, a mixture of solid boron, magnesium oxide, and either tin oxide or iron oxide powders was placed in a graphite crucible which was heated under a nitrogen atmosphere in a vertical induction furnace to 1500 °C. Nitrogen carrier gas brought the reactive vapor resulting from the chemical reactions within the powder mixture into a graphite vessel where it reacted with ammonia to form a white, spongy material rich in BNNTs. The BNNTs used in the present study were synthesized by a different procedure that involved CNTs as a sacrificial material to direct the tubular growth of BN from boron oxide vapor and nitrogen gas.[23] Figure 1b shows a scanning electron microscopy (SEM) image of the precursor BNNTs; as indicated in the previous study, their diameters and lengths are similar to those of starting CNTs.[23] When these CNT-templated BNNTs were treated exactly according to the procedure reported in our previous work[20] (large excess of K, annealing at 300 °C for 72 h), these BNNTs also formed BNNRs through longitudinal splitting, but the amount of split tubes was dramatically different from that observed previously. Figure 1c shows an SEM image of the reaction product. While only ~1%

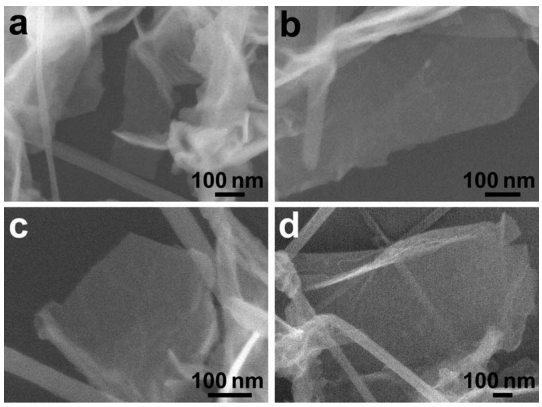

Figure 2. High-magnification SEM images of selected BNNRs from the sample shown in Figure 1c.

of treated BNNTs exhibited splitting in the previous study, nearly all BNNTs used here show some splitting. Because of the folding and entanglement of the numerous BNNRs produced from split nanotubes (Figure 1c), it is difficult to count BNNRs and differentiate between fully split *versus* partially split BNNTs, and thus precisely determining the yield of BNNRs that are completely exfoliated from the parent nanotubes is not possible. This is different from our previous work,[20] where a statistical analysis of potassium-treated samples was substantially easier because of the much lower yield of BNNRs and hence their negligible aggregation.

RESULTS AND DISCUSSION

Due to high degree of splitting and thus a large amount of BNNRs in a sample, the exfoliated BN fragments are mostly entangled (Figure 1c). Representative SEM images of the fragments of non-entangled BNNRs are shown in Figure 2. The ribbons look uniform with no observable contamination or disorder at the basal plane; the edges are mostly straight except for some occasional tears. These BNNRs are semitransparent to the electron beam, as the residual nanotubes covered by the BN sheets are clearly visible, which indicates the thinness of these ribbons.

When BNNRs are deposited from an isopropyl alcohol dispersion onto a Si/SiO_2 substrate for imaging, some of the ribbons are partially or fully suspended because they are mixed with the remaining nanotubes; such ribbons could be easily imaged by SEM. However, when a thin BNNR is placed directly on the silica surface, SEM visualization is difficult because there is a small topographic contrast (only a few nanometers), and there is little electron density difference between the dielectric ribbon and the dielectric substrate. Most of the BNNRs that are imaged by SEM directly on a Si/SiO_2 substrate (such as the ones shown in Figure 2) are >10 nm thick. An example of this effect is shown in Figure 3a that exhibits a long BNNR with very straight parallel edges that is barely visible unlike many other ribbons in this image. The area highlighted by the

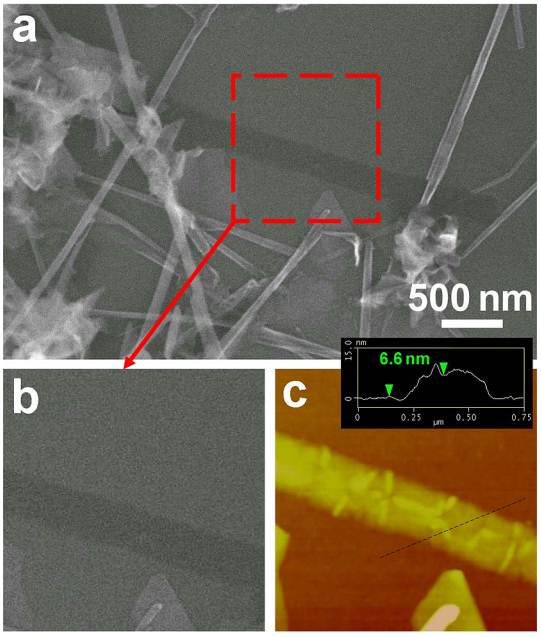

Figure 3. Comparison of SEM and AFM images of BNNRs. (a) SEM image of a BNNR sample showing a long straight ribbon in the center. The area highlighted by the red square was then reimaged by (b) SEM and (c) AFM. The inset in panel (c) shows a height profile along the dashed line.

red square in Figure 3a was imaged by both SEM (Figure 3b) and atomic force microscopy (AFM, Figure 3c). According to the AFM height profile shown in the inset in Figure 3c, this BNNR has a thickness of ~6.6 nm. As we discuss later, it is likely that the layers in this ribbon assume an AA′ stacking that has an interplanar distance of 0.333 nm.[12] This BNNR consists of multiple layers, although it is difficult to precisely determine the number of layers in this ribbon based on the measured AFM height profile, due to the likely presence of some trapped solvent molecules at the BNNR/SiO_2 interface. However, despite its thickness, this BNNR is barely visible in the SEM image regardless of the accelerating voltage (Figure 3a). Occasionally, we observed thinner ribbons by AFM that we could not later find by SEM, suggesting that SEM images like the one shown in Figure 1c could underestimate the amount of thin BNNRs in the samples.

Interestingly, it is straightforward to visualize even monolayer GNRs with comparable dimensions deposited on Si/SiO_2[24−26] due to a substantial difference in conductivities of GNRs and silica. Images of a single GNR captured by both SEM and AFM provide comparable information about the ribbon's morphology.[25] In contrast, in the case of a BNNR on a Si/SiO_2 substrate, AFM resolved some structural features that are not visible by SEM, such as nanoscopic ripples (Figure 3c). The presence of these ripples indicates that few-layer BNNRs are very flexible and could accommodate even a nanoscopic radius of curvature without cracking.

Another powerful tool for the imaging of BNNRs is transmission electron microscopy (TEM). In TEM

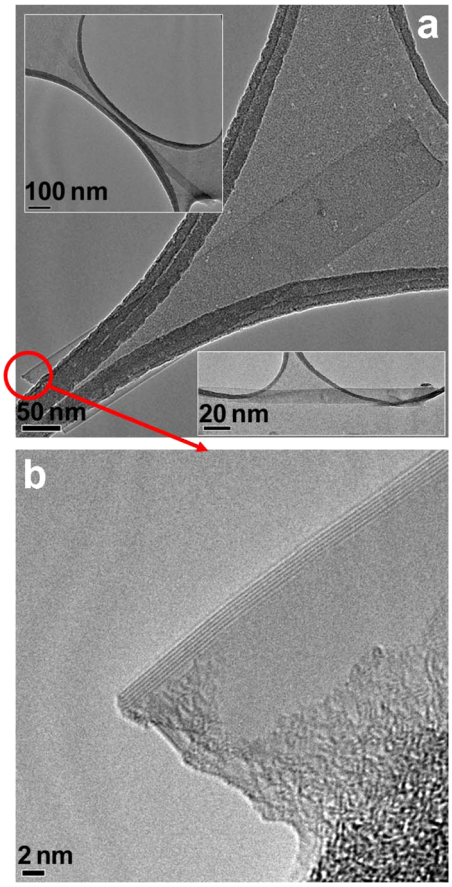

Figure 4. TEM characterization of BNNRs. (a) TEM images of three representative BNNRs. (b) High-resolution TEM image of the edge of a ribbon shown in the center of panel (a).

images, we observed multiple few-layer ribbons with thicknesses ranging from 2 to >10 layers that are completely delaminated from the parent nanotubes; many of these ribbons have very straight parallel edges. Three representative BNNRs are shown in Figure 4a. Figure 4b shows a high-resolution TEM image of the edge of a ribbon shown in Figure 4a, demonstrating that this particular ribbon is 6 layers thick. As will be discussed later, many BNNRs observed in TEM images are entangled and folded, so it is difficult to estimate their length and aspect ratio distributions, but for select straight and isolated BNNRs, these characteristics are noteworthy. Many BNNRs observed in this study had lengths in the micrometer range and aspect ratios >30 (see the top inset in Figure 4a).

Interpretation of TEM results should be done with care because some flattened BN structures observed by TEM could represent collapsed BNNTs and not BNNRs. Partial flattening and complete collapsing have been previously observed in TEM studies of both carbon and BN nanotubes.[27,28] One such collapsed BNNT can be observed in Figure 5a, in which the black arrows show that flattening occurs at both ends of a BNNT, which retains its tubular shape in the middle. A higher resolution TEM image of the same BNNT (Figure 5b)

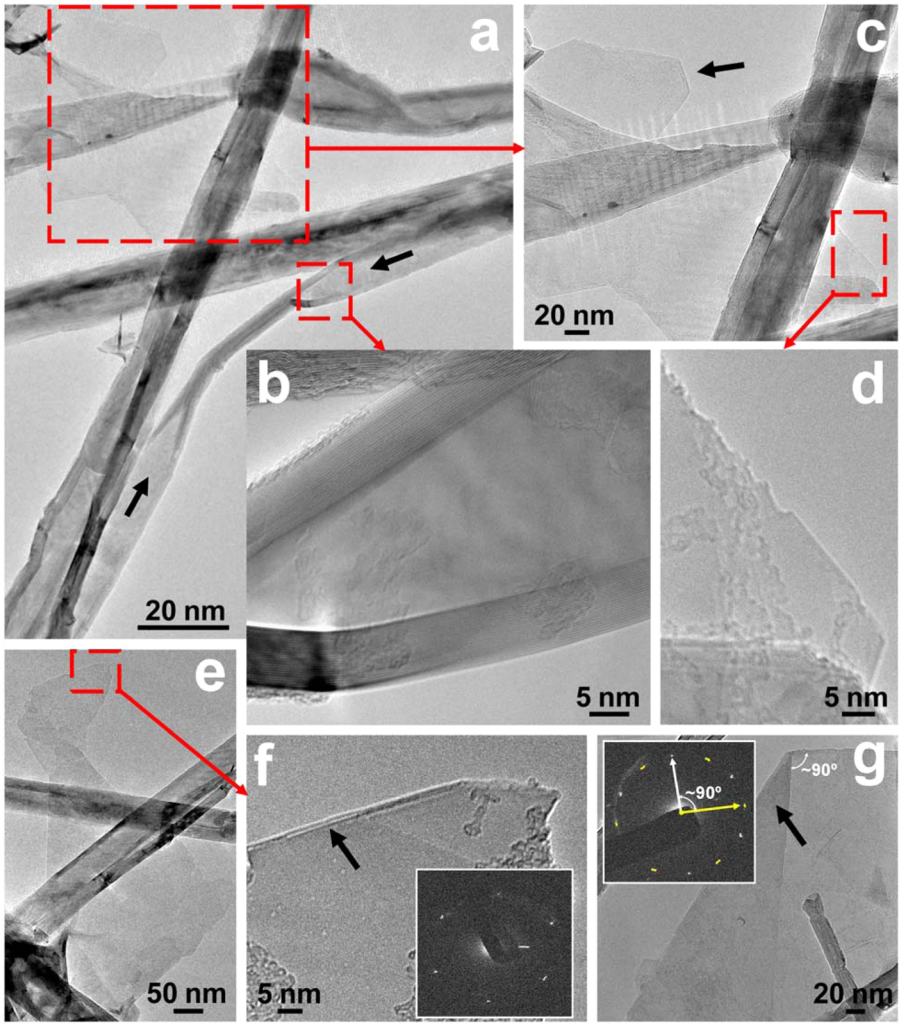

Figure 5. TEM images of BNNRs. (a) TEM image of a BNNT with both ends collapsed, as indicated by the black arrows. The higher magnification images of the areas highlighted by red dashed squares are presented in panels (b) and (c). (d) TEM image of a monolayer fragment of a BNNR highlighted by the red dashed square in panel (c). (e) TEM image of a folded bilayer BNNR. The higher magnification image of the highlighted area along with the corresponding electron diffraction pattern is shown in panel (f). (g) TEM image of a folded multilayered BNNR and the corresponding electron diffraction pattern. One set of six spots in the diffraction pattern is highlighted by yellow. See text for further details.

shows that this particular nanotube consists of more than 20 shells. According to geometrical considerations, if collapsed parts of a BNNT are perpendicular to the electron beam, their widths should be larger than the diameter of a tubular portion of the BNNT by the factor of $\sim\pi$ (or less in case of only partial flattening or a tilted view). In contrast, the BNNRs should be wider than the diameters of the parent BNNTs by the factor of $\sim 2\pi$. Such a wider but thinner BN structure could be observed in the top left part of Figure 5a. Figure 5c shows that this fragment of a TEM grid contains at least two folded BNNRs. During the sonication in isopropyl alcohol, different shells of BNNRs could exfoliate,[29] resulting in BNNRs that are only a few layers thick. Higher magnification images show that the ribbon indicated by the black arrow consists of 5 layers. Another ribbon in this image that is highlighted by the red dashed square is a monolayer (Figure 5d), which demonstrates that monolayer BNNRs can be produced by the disclosed method.

Figure 5e shows another thin BNNR with multiple folds. A higher magnification TEM image shows that this is a bilayer ribbon, as indicated by the black arrow in Figure 5f. Interestingly, the electron diffraction pattern recorded for the BNNR area shown in this image exhibits only six distinct diffraction spots; see the inset in Figure 5f. This indicates that the material is highly crystalline and also that the two layers in this BNNR have the same crystallographic orientation.[30] This and similar six-fold diffraction patterns recorded for other multilayered ribbons demonstrate that the AA′ stacking typical for different shells in BNNTs is inherited by the layers of BNNRs.

This AA′ stacking observation is consistent with the splitting mechanism that was proposed in our previous work.[20] Different shells of multiwalled BNNTs experience significantly stronger interplanar interaction compared to the shells in multiwalled CNTs due to polar attraction of boron and nitrogen atoms. Heteroatoms

from adjacent shells align, resulting in AA′ stacking between planes of BNNTs, which is different from CNTs where different walls could have random chiralities.[31] However, the commensurate AA′ stacking of different shells in a BNNT cannot continue around the full circumference of a nanotube due to the changing diameter of concentric tube walls. A detailed TEM diffraction study revealed that this mismatch is compensated by the paths of strained sp^3 bonds that run parallel to the longitudinal axis of the nanotube.[32] As we proposed previously, the potassium atoms could preferentially intercalate near these higher energy paths of sp^3 bonds, eventually resulting in splitting along these paths.[20] If the proposed splitting mechanism is correct, the resulting BNNR should mostly be multilayer (because the polar interaction between boron and nitrogen atoms from adjacent shells of BNNTs should also result in attraction of the BNNR layers that will have the same AA′ stacking) and have straight parallel edges. Both of these features are observed experimentally; see TEM images in Figures 4 and 5.

Also, on the basis of the proposed mechanism of splitting, we previously theorized that most BNNRs produced by the potassium-induced splitting of BNNTs should have either zigzag or armchair edges as opposed to other edge orientations.[20] For the BNNR shown in Figure 5f, from the comparison of the TEM image and the electron diffraction pattern, we can conclude that the edge indicated by the black arrow is predominantly zigzag, which is again in agreement with the proposed splitting mechanism.

For some multilayered BNNRs, we observed electron diffraction patterns with multiple six-fold diffraction sets. However, since many ribbons drape along the lacey carbon in a TEM grid and form multiple folds, it is often difficult to determine whether such diffraction patterns indicate random stacking of layers in a BNNR or simply the folding of a ribbon. An example of a folded fragment of a multilayered BNNR is shown in Figure 5g. The ribbon is folded by ~90°, and the electron diffraction pattern recorded for the folded area indicated by the black arrow also shows two sets of six-fold diffraction spots rotated by ~90° relative to each other (see the inset in Figure 5g). Therefore, this is likely a multilayered ribbon with AA′ stacking for which two sets of six-fold diffraction spots simply indicate the angle of folding. For some BNNRs, it was not clear whether the recorded 12- or 18-fold diffraction patterns indicate random orientations of BN layers or folding because in some TEM images the number of individual ribbons and the folding edges are not clearly visible (see Figure 5c, for example). Yet, our TEM data indicate that the majority of multilayerd BNNRs have an AA′ stacking of layers that is inherited from BNNTs.

Finally, we performed a series of experiments aimed to optimize the synthesis of BNNRs. First, we found that, for the precursor BNNTs used in work, it was not necessary to run the reaction for 72 h as in our original study with different BNNTs;[20] a high yield of BNNRs could be achieved after 12 h of reaction. Also, we originally performed the annealing of a BNNT/K mixture in quartz tubes that are reliable but rather expensive and difficult to process. We found that the synthesis of BNNRs could be performed in glass ampules that are less expensive and easier to work with, as glass melts at lower temperatures than quartz. The most convenient and inexpensive reactors used in this study were glass ampules made from disposable Pasteur pipets that, in addition to other advantages, allow running multiple syntheses of BNNRs at different conditions on a very small scale.

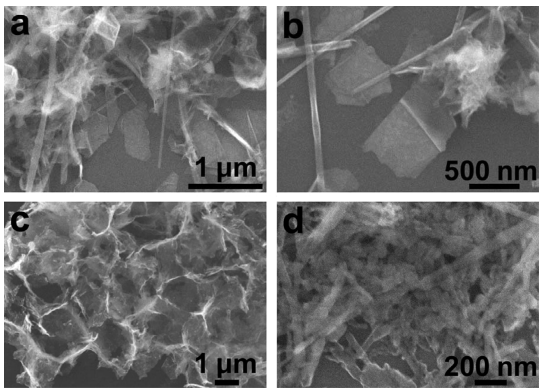

Figure 6. SEM images of the BNNR products obtained at (a,b) 350 °C and (c,d) 450 °C.

We also investigated the effect of the temperature of potassium intercalation on the yield of BNNRs and their structural quality. Figure 6a,b shows representative SEM images of a BNNR product obtained at 350 °C. These images demonstrate that the BNNRs are obtained at even a higher yield comparable to that at 300 °C; they look uniform and have well-defined edges (Figure 6b), as discussed previously, with few tubular structures remaining. The BNNR product obtained at 450 °C appears to be even better exfoliated and contains a smaller number of residual BNNTs (Figure 6c). However, higher magnification SEM images show the presence of a disordered BN material (Figure 6d), suggesting that vigorous potassium-induced splitting at higher temperatures results in structural damage to the resulting BNNRs. Therefore, the 300−350 °C temperature range appears to be optimal for the synthesis of BNNRs from BNNTs prepared as described here.[23] However, since BNNT materials prepared by different techniques[22,23] exhibit such different reactivities in the discussed potassium-induced splitting reaction, it is possible that the optimum synthetic temperature could vary for BN materials produced using other methods.

CONCLUSION

In summary, we demonstrate that potassium-induced splitting of BNNTs is a high-yielding method

to obtain bulk quantities of high-quality BNNRs; nearly all nanotubes exhibit splitting if a proper precursor material is chosen. The resulting BNNRs are highly crystalline; many of them have a high aspect ratio and straight parallel edges. The ribbons are produced at moderate temperature (300−350 °C) using inexpensive glass ampules. After the synthesis, the BNNRs could be dispersed in isopropyl alcohol[29] and then deposited on any substrate, such as a silicon wafer or a TEM grid, for further studies. The microscopy analysis provides some insights into the mechanism of the formation of BNNRs from BNNTs. The discussed mechanism favors the formation of multilayered BNNRs with all layers having parallel edges. Few-layered and even monolayer ribbons could be obtained from multilayered BNNRs by a solution exfoliation.[29]

An important fundamental result of this study is that BNNTs prepared by different synthetic approaches could exhibit dramatically different reactivities in the present potassium splitting reaction: the yield of BNNRs could be as low as 1%[20] or nearly 100% depending on the nanotube precursor material.[22,23] Thus, this work demonstrates the need for future comparison studies of BN nanomaterials synthesized using different approaches to better understand their preparation-dependent physical and chemical properties.

EXPERIMENTAL SECTION

Although several reactions were performed in 1/4 in. quartz tubes as described in the previous work,[20] we typically performed the reactions on a very small scale using 146 mm long disposable glass Pasteur pipets (Fisherbrand) to make the reaction ampules. A tapered end of a pipet was first sealed using an acetylene torch and then filled with a few cubic millimeters of BNNTs (due to the low-density spongy nature of this material, this accounts for less than 0.5 mg, so the precise determination of the mass was not possible with a standard analytical balance). Then, a large excess of the potassium metal (>30 mg), which was freshly cut in a fume hood and rinsed with dry diethyl ether to remove the mineral oil, was added to the ampule **(CAUTION: Potassium and sealing of the potassium-loaded ampule should be handled with utmost care due to the highly reactive nature of potassium metal. Users should wear safety glasses and a face shield, and all operations should be done in a fume hood when handling these materials)**. The ampule was evacuated to $\sim 10^{-3}$ Torr and sealed with an acetylene torch. Then, the BNNT/K mixture was annealed at 300 to 450 °C for 12 to 72 h, cooled to room temperature, and then quenched with ethanol. The resulting material was washed with 2 mL of 5 wt % HF aqueous solution and with an excess of water to remove possible silicate impurities left from the glass ampule **(CAUTION: HF is highly corrosive and should be handled with utmost care)**. Residual carbonaceous materials, presumably from remaining mineral oil and from atmospheric adsorbates, graphitized on the surface of the BN material during the treatment, making it grayish. This residual carbon was therefore removed by annealing at 600 °C in air for 30 min to form a white BN material.

The BNNR products as well as the precursor BNNTs could be readily dispersed in isopropyl alcohol under mild sonication[29] and then deposited on a substrate followed by solvent evaporation. For the SEM and AFM studies, BNNTs and BNNRs were deposited on Si/SiO_2 substrates (SQI; 300 nm thick thermal SiO_2 on a heavily p-doped Si). For the TEM analysis, BNNRs were deposited on Au mesh lacey carbon TEM grids (Ted Pella). SEM imaging was performed on a JEOL-6500 field-emission microscope. AFM images were obtained using a Digital Instruments Nanoscope IIIa, operating in tapping mode; we used Si tips *n*-doped with 1 to 10 Ω·cm phosphorus (Veeco) at a 0.5 Hz and a 512 × 512 resolution. TEM and electron diffraction analysis were performed using a JEOL 2010 microscope. Figure 1a was prepared using Accelrys Materials Studio 4.3.

Conflict of Interest: The authors declare no competing financial interest.

Acknowledgment. This work was supported in part by the Air Force Research Laboratory through University Technology Corporation (09-S568-064-01-C1); the Air Force Office of Scientific Research (FA9550-09-1-0581); the Office of Naval Research MURI Graphene Program (N00014-09-1-1066); the Director, Office of Energy Research, Office of Basic Energy Sciences, Materials Sciences and Engineering Division, of the U.S. Department of Energy under Contract No. DE-AC02-05CH11231, which provided for student support and detailed TEM and SEM characterization; and the Center of Integrated Nanomechanical Systems under NSF Grant EED-0832819, which provided for staff support. D.G. acknowledges support from the NIMS Grant No. BE063. A.S. also acknowledges support from the NSF through Nebraska MRSEC (DMR-0820521) and EPSCoR (EPS-1004094).

REFERENCES AND NOTES

1. Barone, V.; Peralta, J. E. Magnetic Boron Nitride Nanoribbons with Tunable Electronic Properties. *Nano Lett.* **2008**, *8*, 2210–2214.
2. Park, C. H.; Louie, S. G. Energy Gaps and Stark Effect in Boron Nitride Nanoribbons. *Nano Lett.* **2008**, *8*, 2200–2203.
3. Zheng, F. W.; Zhou, G.; Liu, Z. R.; Wu, J.; Duan, W. H.; Gu, B. L.; Zhang, S. B. Half Metallicity Along the Edge of Zigzag Boron Nitride Nanoribbons. *Phys. Rev. B* **2008**, *78*, 205415.
4. Chen, W.; Li, Y. F.; Yu, G. T.; Zhou, Z.; Chen, Z. F. Electronic Structure and Reactivity of Boron Nitride Nanoribbons with Stone-Wales Defects. *J. Chem. Theory Comput.* **2009**, *5*, 3088–3095.
5. Topsakal, M.; Akturk, E.; Ciraci, S. First-Principles Study of Two- and One-Dimensional Honeycomb Structures of Boron Nitride. *Phys. Rev. B* **2009**, *79*, 115442.
6. Lai, L.; Lu, J.; Wang, L.; Luo, G. F.; Zhou, J.; Qin, R.; Gao, Z. X.; Mei, W. N. Magnetic Properties of Fully Bare and Half-Bare Boron Nitride Nanoribbons. *J. Phys. Chem. C* **2009**, *113*, 2273–2276.
7. Ding, Y.; Wang, Y. L.; Ni, J. The Stabilities of Boron Nitride Nanoribbons with Different Hydrogen-Terminated Edges. *Appl. Phys. Lett.* **2009**, *94*, 233107.
8. Wang, Y. L.; Ding, Y.; Ni, J. Fluorination-Induced Half-Metallicity in Zigzag Boron Nitride Nanoribbons: First-Principles Calculations. *Phys. Rev. B* **2010**, *81*, 193407.
9. Lopez-Bezanilla, A.; Huang, J. S.; Terrones, H.; Sumpter, B. G. Boron Nitride Nanoribbons Become Metallic. *Nano Lett.* **2011**, *11*, 3267–3273.
10. Chen, W.; Li, Y. F.; Yu, G. T.; Li, C. Z.; Zhang, S. B. B.; Zhou, Z.; Chen, Z. F. Hydrogenation: A Simple Approach To Realize Semiconductor−Half-Metal−Metal Transition in Boron Nitride Nanoribbons. *J. Am. Chem. Soc.* **2010**, *132*, 1699–1705.
11. Tang, S. B.; Cao, Z. X. Structural and Electronic Properties of the Fully Hydrogenated Boron Nitride Sheets and Nanoribbons: Insight from First-Principles Calculations. *Chem. Phys. Lett.* **2010**, *488*, 67–72.
12. Lin, Y.; Connell, J. W. Advances in 2D Boron Nitride Nanostructures: Nanosheets, Nanoribbons, Nanomeshes, and Hybrids with Graphene. *Nanoscale* **2012**, *4*, 6908–6939.
13. Kosynkin, D. V.; Higginbotham, A. L.; Sinitskii, A.; Lomeda, J. R.; Dimiev, A.; Price, B. K.; Tour, J. M. Longitudinal

Unzipping of Carbon Nanotubes To Form Graphene Nanoribbons. *Nature* **2009**, *458*, 872–876.
14. Jiao, L. Y.; Zhang, L.; Wang, X. R.; Diankov, G.; Dai, H. J. Narrow Graphene Nanoribbons from Carbon Nanotubes. *Nature* **2009**, *458*, 877–880.
15. Cano-Marquez, A. G.; Rodriguez-Macias, F. J.; Campos-Delgado, J.; Espinosa-Gonzalez, C. G.; Tristan-Lopez, F.; Ramirez-Gonzalez, D.; Cullen, D. A.; Smith, D. J.; Terrones, M.; Vega-Cantu, Y. I. Ex-MWNTs: Graphene Sheets and Ribbons Produced by Lithium Intercalation and Exfoliation of Carbon Nanotubes. *Nano Lett.* **2009**, *9*, 1527–1533.
16. Sinitskii, A.; Fursina, A. A.; Kosynkin, D. V.; Higginbotham, A. L.; Natelson, D.; Tour, J. M. Electronic Transport in Monolayer Graphene Nanoribbons Produced by Chemical Unzipping of Carbon Nanotubes. *Appl. Phys. Lett.* **2009**, *95*, 253108.
17. Jiao, L. Y.; Wang, X. R.; Diankov, G.; Wang, H. L.; Dai, H. J. Facile Synthesis of High-Quality Graphene Nanoribbons. *Nat. Nanotechnol.* **2010**, *5*, 321–325.
18. Kosynkin, D. V.; Lu, W.; Sinitskii, A.; Pera, G.; Sun, Z. Z.; Tour, J. M. Highly Conductive Graphene Nanoribbons by Longitudinal Splitting of Carbon Nanotubes Using Potassium Vapor. *ACS Nano* **2011**, *5*, 968–974.
19. Zeng, H. B.; Zhi, C. Y.; Zhang, Z. H.; Wei, X. L.; Wang, X. B.; Guo, W. L.; Bando, Y.; Golberg, D. "White Graphenes": Boron Nitride Nanoribbons *via* Boron Nitride Nanotube Unwrapping. *Nano Lett.* **2010**, *10*, 5049–5055.
20. Erickson, K. J.; Gibb, A. L.; Sinitskii, A.; Rousseas, M.; Alem, N.; Tour, J. M.; Zettl, A. K. Longitudinal Splitting of Boron Nitride Nanotubes for the Facile Synthesis of High Quality Boron Nitride Nanoribbons. *Nano Lett.* **2011**, *11*, 3221–3226.
21. Li, L.; Li, L. H.; Chen, Y.; Dai, X. J.; Lamb, P. R.; Cheng, B.-M.; Lin, M.-Y.; Liu, X. High-Quality Boron Nitride Nanoribbons: Unzipping during Nanotube Synthesis. *Angew. Chem., Int. Ed.* **2013**, *52*, 4212–4216.
22. Zhi, C.; Bando, Y.; Tan, C.; Golberg, D. Effective Precursor for High Yield Synthesis of Pure BN Nanotubes. *Solid State Commun.* **2005**, *135*, 67–70.
23. Han, W.; Bando, Y.; Kurashima, K.; Sato, T. Synthesis of Boron Nitride Nanotubes from Carbon Nanotubes by a Substitution Reaction. *Appl. Phys. Lett.* **1998**, *73*, 3085–3087.
24. Sinitskii, A.; Dimiev, A.; Kosynkin, D. V.; Tour, J. M. Graphene Nanoribbon Devices Produced by Oxidative Unzipping of Carbon Nanotubes. *ACS Nano* **2010**, *4*, 5405–5413.
25. Sinitskii, A.; Dimiev, A.; Corley, D. A.; Fursina, A. A.; Kosynkin, D. V.; Tour, J. M. Kinetics of Diazonium Functionalization of Chemically Converted Graphene Nanoribbons. *ACS Nano* **2010**, *4*, 1949–1954.
26. Sinitskii, A.; Kosynkin, D. V.; Dimiev, A.; Tour, J. M. Corrugation of Chemically Converted Graphene Monolayers on SiO_2. *ACS Nano* **2010**, *4*, 3095–3102.
27. Chopra, N. G.; Benedict, L. X.; Crespi, V. H.; Cohen, M. L.; Louie, S. G.; Zettl, A. Fully Collapsed Carbon Nanotubes. *Nature* **1995**, *377*, 135–138.
28. Golberg, D.; Bando, Y.; Bourgeois, L.; Kurashima, K.; Sato, T. Insights into the Structure of BN Nanotubes. *Appl. Phys. Lett.* **2000**, *77*, 1979–1981.
29. Coleman, J. N.; Lotya, M.; O'Neill, A.; Bergin, S. D.; King, P. J.; Khan, U.; Young, K.; Gaucher, A.; De, S.; Smith, R. J.; *et al.* Two-Dimensional Nanosheets Produced by Liquid Exfoliation of Layered Materials. *Science* **2011**, *331*, 568–571.
30. Kim, K.; Lee, Z.; Regan, W.; Kisielowski, C.; Crommie, M. F.; Zettl, A. Grain Boundary Mapping in Polycrystalline Graphene. *ACS Nano* **2011**, *5*, 2142–2146.
31. Golberg, D.; Bando, Y.; Tang, C. C.; Zhi, C. Y. Boron Nitride Nanotubes. *Adv. Mater.* **2007**, *19*, 2413–2432.
32. Celik-Aktas, A.; Zuo, J. M.; Stubbins, J. F.; Tang, C. C.; Bando, Y. Double-Helix Structure in Multiwall Boron Nitride Nanotubes. *Acta Crystallogr., Sect. A: Found. Crystallogr.* **2005**, *61*, 533–541.